

Active Cheerios: 3D-Printed Marangoni-Driven Active Particles at an Interface

Jackson K. Wilt^{*1,2}, Nico Schramma¹, Jan-Willem Bottermans¹, and Maziyar Jalaal^{†1}

¹*Van der Waals-Zeeman Institute, Institute of Physics,*

University of Amsterdam, Science Park 904, Amsterdam, 1098XH, The Netherlands

²*John A. Paulson School of Engineering and Applied Sciences, Harvard University, Cambridge, MA 02138, USA*

Marangoni surfers are simple, cost-effective tabletop experiments that, despite their simplicity, exhibit rich dynamics and collective behaviors driven by physicochemical mechanisms, hydrodynamic interactions, and inertial motion. This work introduces self-propelled particles designed and manufactured through 3D printing to move on the air-water interface. We develop particles with tunable motility and controlled particle-particle interactions by leveraging surface tension-mediated forces, such as the Marangoni effect for propulsion and the Cheerios effect for interactions. Rapid prototyping through 3D printing facilitates the exploration of a wide design space, enabling precise control over particle shape and function. We exemplify this by creating translational and chiral particles. Additionally, we investigate self-assembly in this system and highlight its potential for modular designs where mechanically linked particles with varying characteristics follow outlined trajectories. This research offers a flexible, low-cost approach to designing active interfacial systems and opens new possibilities for further advancements of adaptive, multifunctional devices.

Keywords: Active Particles | Marangoni Surfers | Active Matter | Cheerios Effect

I. INTRODUCTION

Novel propulsion methods for devices moving on fluid interfaces have generated remarkable interest in engineering applications such as chemical delivery, environmental monitoring, and robotic systems [1–8]. While many interfacial devices and living organisms use mechanical forces in fluids to move, several studies have shown that using physicochemical processes at the interface instead proves an effective method to move objects across scales [9–11]. A notable phenomenon in this category is the Marangoni effect, where a surface tension gradient leads to mechanical work [12]. The Marangoni effect has been known since (at least) the mid 1800s [13, 14], and its utilization by various water-dwelling insects has also been discovered over a century ago [9]. More recently, various types of synthetic active particles self-propelled by the Marangoni effect and flow have been studied. Examples include colloids and micro-droplets [15–18], as well as camphor boats [19–24] and bio-mimetic swimming devices [25, 26]. Such “particles” break the symmetry with the gradient of surface tension and create a persistent Marangoni self-propulsion lifetime.

Like many other active systems, precise motility control of Marangoni-driven self-propelled particles is still an open challenge, often due to restrictive fuel properties or design constraints. Previous efforts include changing the shape of the Marangoni surfers [27, 28], controlled release of the fuel [29], an external electric field [30] and locally changing the properties of the surface [31]. Yet, a generic framework to design Marangoni-driven particles with tunable motility and particle-particle interactions offers a broad scope for future work. We aim to address this by proposing a simple and frugal system of active particles made by additive manufacturing. Our study is strongly influenced by works typically known for educational purposes, such as studies using household dish soaps and alcohol as fuel. In the case of the colloquially called “soap boats,” studies use liquid soap released onto the surface of the water as a powerful surfactant-induced Marangoni effect in classroom demonstrations [32]. While soap boats create significant propulsion, the surfactants rapidly saturate the water surface, thus equilibrating the surface tension gradient in very short time spans. An alternative, using common products with rapid diffusion, is ethanol [33, 34]. Particles using ethanol solutions as fuel, in one instance, are referred to as “cocktail boats”, where an alcohol-driven edible boat was created [34]. While both the soap and cocktail boats in the literature are well regarded, they are not designed or investigated for their complex motion. We develop an alcohol (Marangoni)-driven active system following the notion of low cost and accessibility. Meanwhile, we provide an experimental framework to study active particles across a wide range of hydrodynamical regimes, such as inertial active particles, which have received much less attention [35, 36].

Our system also utilizes particle-particle interfacial interactions generated from liquid deformation due to the particles. The interface curvature at the particles has shown substantial attraction forces on centimeter-scale

*jacksonwilt@g.harvard.edu, ORCID: 0000-0002-0023-4566

†m.jalaal@uva.nl, ORCID: 0000-0002-5654-8505

objects and surface-dwelling insects [9, 37]. This interaction between unconstrained inertial agents, mediated by the surface tension, similar to our system, is best described by the ‘‘Cheerios effect’’, which refers to the clustering behavior observed in floating cereal in a bowl of milk [38]. The attractive (and repulsive) forces of the Cheerios effect depend highly on the meniscus shape at the solid-fluid interface, governed by material surface properties (hydrophobicity, hydrophilicity) and geometry.

We create our particles with rapid prototyping (3D printing) to efficiently test the space of possible designs. Specifically, the control of fuel deposition is important for the Marangoni effect and the particle geometry for the Cheerios effect. We design simple centimeter-scale buoy-like particles operated by Marangoni-driven thrust to locomote on an air-water interface. We explore a range of surface tension gradients by varying ethanol concentration [39] and lowering the surface tension of the fuel mixture, during which we monitor the particle motility and average movement life spans via tracking. Extending the use of 3D-printing, we explore the concept of chiral particles [40–43] and present a Marangoni-driven chiral spinners on the liquid surface. Finally, we show how the present system can benefit modularity, where particles can be linked mechanically to design a geometry with a desirable trajectory.

II. MARANGONI-DRIVEN ACTIVE PARTICLES DESIGN AND MOTILITY

Our active particles are, in principle, a type of self-propelled motor that uses an onboard water-ethanol fuel reservoir and one or multiple small outlets to produce Marangoni-induced forces on a water surface. The surface motors have a buoyant air-filled base, a conical fuel reservoir, one or more fuel release outlets, and a tracking cap (see Fig. 1a).

Each particle is designed using computer-aided design software (SolidWorks) and exported as a 3D model file to be 3D-printed and assembled, seen in Fig. 1b, for deployment onto the water surface (see Appendix A for the details of materials used). The tracking caps (blue and green circles) are also 3D printed as an extra module and are attached to the top. In single-outlet particles, the blue circle is located on the side of the particle with the fuel outlet, so one can track the orientation of the particle with respect to the outlet position. A simple tracking setup, consisting of a camera located on top of the water basin and particle detection analysis, tracked the position and rotation of the particle through open-source Python packages OpenCV [44] and TrackPy [45]. Particles maneuver in a circular domain (45 cm diameter in Fig. 1). The black containment rings (also 3D printed) are affixed to the bottom of a much larger water basin (150 cm \times 150 cm). The ring is 3 mm taller than the water depth of 3 cm so the dissolution of the fuel is retained if not evaporated; because of this, the ring is removed and replaced after each consecutive test to avoid the accumulation of ethanol however with the largest ring (45 cm) the ring is left in place. For optimal repulsion of boundaries and particles, the containment rings are treated with a super-hydrophobic surface coating (NeverWet spray). The combination of a hydrophobic ring and a hydrophilic particle prevents attractive forces between the two, and hence, the rings act like a repulsive wall (see Appendix B). This allows for long measurements of the freely moving particles, avoiding attractive particle-boundary (solid-solid) interactions that could impede their mobility.

The buoyancy of the particles is designed such that the outlets of 500 μm are positioned at the water-air interface (see Fig. 1a). Both direct forcing at the contact line of the particle and Marangoni flow thrust generated at the nozzle play an important role in the particle propulsion (see Appendix C for simple calculations). The fuel (ethanol-water solution) initially exits the tank from this outlet mainly via the capillary actions. Once it arrives at the air-water interface, the fuel changes the local surface tension of the surrounding environment and creates a continuous mass flow rate. The fuel ejection was visualized by adding 0.1% fluorescein dye to the fuel mixture and illuminating the basin with a low-power UV-blacklight (see Fig. 1c for such a visualization for 50% ethanol fuel). A fast flow regime near the outlet is observed, and the fuel plumes show the surface flow generated and surround the fueled motor. Note that the dye concentration can only correlate well with the fuel concentration at the early time of the release, as ethanol evaporates rapidly and leaves the dye in the water basin. We, therefore, use these experiments for demonstrations of initial flow structures only.

To start, we focus on a single outlet design (see Supplementary Video 1 for an example). Fig. 1d shows a typical trajectory and speed of a particle with 50% ethanol solution as fuel. Driven by the surface tension gradient, the particles generally show ballistic motion while spinning over their lifetimes. The ballistic motion is expected, given the size and magnitude of the forces in our system. The origin of spinning is most likely akin to the persistently broken symmetry at the point of fuel ejection (also see Appendix D for the angular lag). Nonetheless, the characteristics of this broken symmetry and the associated hydrodynamics are to be fully characterized in future studies. The particles’ trajectories are constrained and repelled by the hydrophobic containment ring (45 cm diameter in the example shown in Fig. 1d and e), proving the effectiveness of the strategy used to control the particle-boundary interactions. The higher speeds of the particles are at the beginning of their lifetimes when higher path curvatures are also observed. As the fuel depletes, the speed of the particle decreases, and the path curvature decreases. Meanwhile, the angular velocity (shown in Fig. 1e for

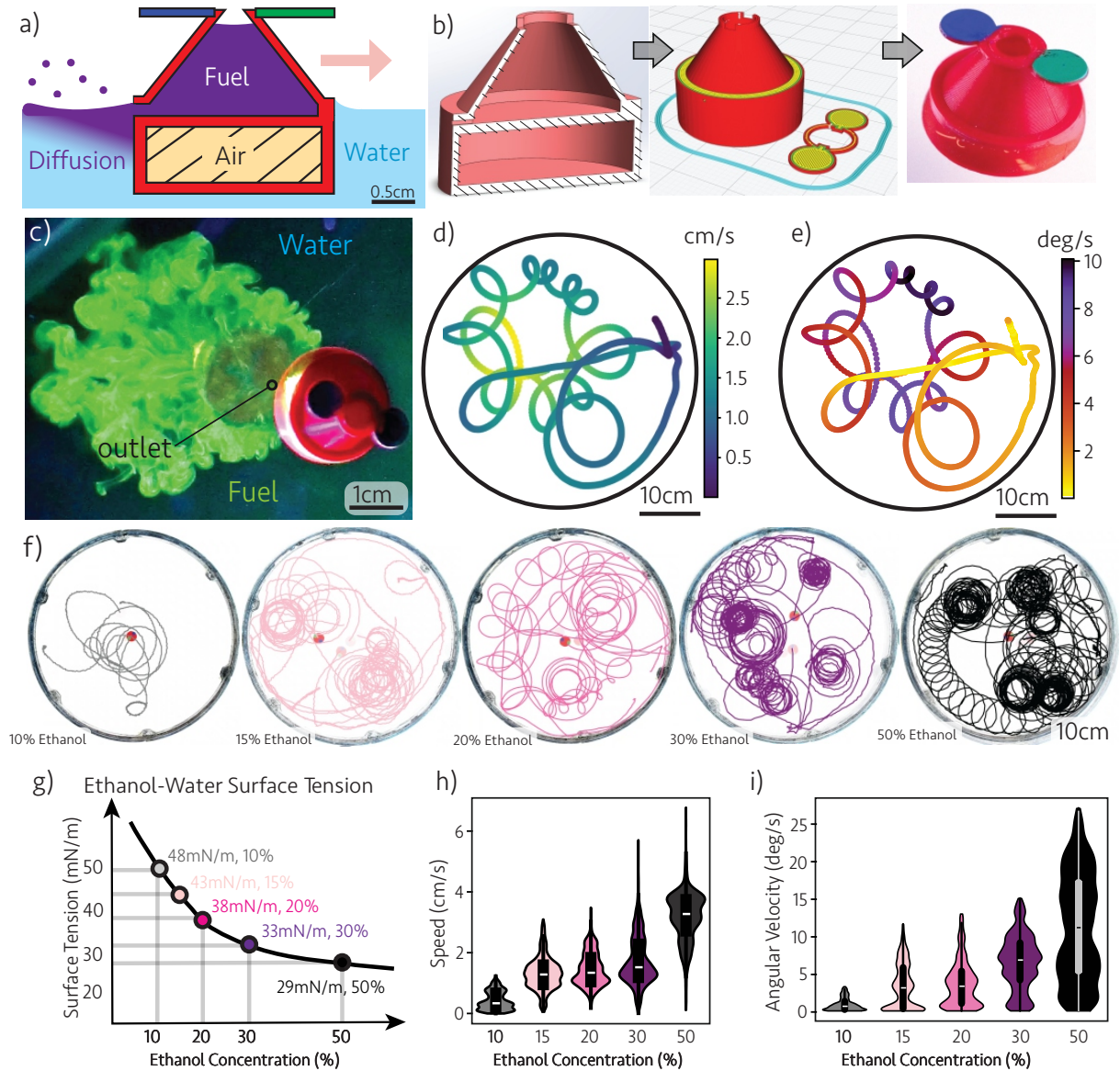


Fig. 1: Marangoni-driven particle design concept, fabrication, and propulsion mechanics: a) Conceptual design cross-section of the particle. b) Process for 3D design, G-code slicing, and 3D printed final design. c) The particle releases the fluorescent-labeled fuel and self-propels on the surface. d) The trajectory of a single-outlet 50% ethanol-powered particle. The color shows the instantaneous speed of the particle. e) Same as in panel d, but the color shows the instantaneous magnitude of angular velocity. f) Single outlet particle trajectories ($n = 3$) with 10%, 15%, 20%, 30%, and 50% ethanol fuel concentrations. g) The corresponding surface tension relationships between fuel types (values adopted from [39]). h) Speed distribution for various ethanol concentrations. i) The angular velocity distribution for various ethanol concentrations.

the same trajectory) also decreases as the particle depletes its fuel, which is closely related to the reorientation associated with the small loops formed from spinning.

We modulate the thrust output from the particle using various ethanol concentrations, which modify the surface tension of the fuel (see Fig. 1g). We test multiple ethanol-water fuels by mixing deionized water at weight concentrations of 10%, 15%, 20%, 30%, and 50% ethanol. Selected trajectories ($n = 3$) for these pictures are shown in Fig. 1f. The ballistic and spiraling characteristics through movement are observed for all fuel constituents. The frequency and characteristic size of each spiral, however, correlate with ethanol concentration, with more spiraling occurring at higher concentrations of ethanol. As the ethanol concentration increases, we see greater distance traveled with more prominent spiraling characteristics and higher path curvature. The concentration of ethanol controls surface tension (Fig 1g) and, therefore, the motion characteristics of the Marangoni-driven particle. Panels h and i in Fig. 1 show the distribution of speed and angular velocity for the range of ethanol concentrations used here for particles with single outlets. Both quantities feature a wide distribution of values as particles experience a complex trajectory and also interact with the circular containment wall. However, both the average translational speed ($\sim \mathcal{O}(1 \text{ cm/s})$) and angular velocity ($\sim \mathcal{O}(1 - 10 \text{ deg/s})$) of the particles increases with increases in ethanol concentration (*i.e.*, increasing the surface tension gradient).

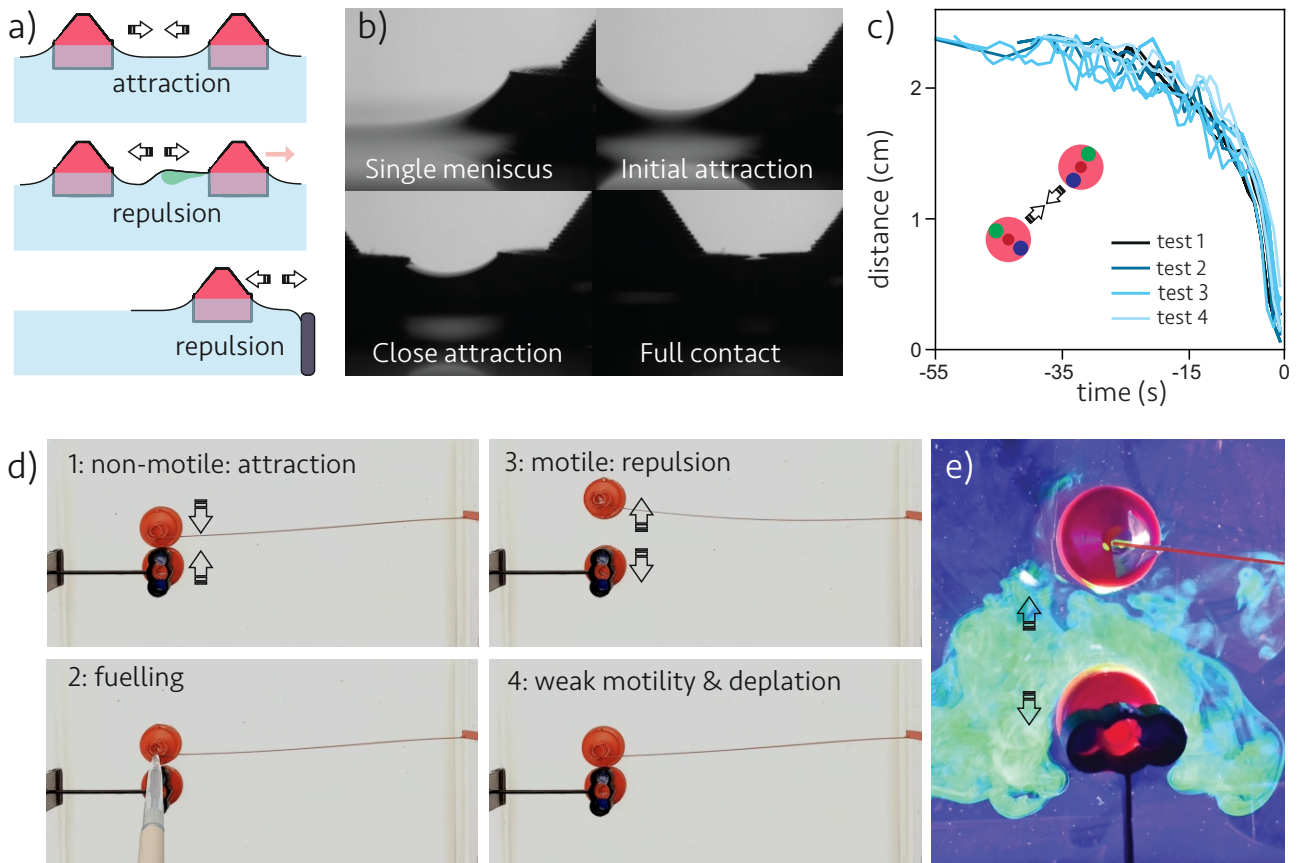


Fig. 2: Particle interactions on the water surface. a) Hydrophilic particles attract each other on the surface, while an active particle avoids and potentially repels other particles. Meanwhile, a hydrophobic wall repels the particles. b) Side view of two particles attached by deformed interfaces (Cheerios effect). c) The distance between two particles for multiple tests, initially positioned at different locations. d) A demonstration of particle interactions. The top particle is attached to a flexible cantilever, while the bottom particle is fixed in position with a stiff (black) cantilever. Initially, non-motile particles are attached to each other when they are close enough. When the top particle is activated by injecting fuel, the particles repel each other via hydrodynamic forces. Eventually, when the motility weakens, and the fuel is depleted, the Cheerios forces dominate again, and the particles attract each other (see Supplementary Video 3). e) Visualization of the onset of Marangoni flow and repulsion. The bottom particle is unpowered and fixed at its position, while the top particle is attached to the cantilever and fueled with 0.1% fluorescein dye in a 30% ethanol-water mixture.

III. MULTI-BODY SYSTEMS: ATTRACTION & REPULSION IN ACTIVE CHEERIOS

After tracking single-motor motility, we investigate the attractive and repulsive forces of a two-body system. It is well-known that two bodies positioned on a fluid interface can interact because of the surface deformations they cause [38, 46–48]. Here, the attractive force between the two particles stems from similar hydrophilic particle surfaces. In contrast, the repulsive forces result from the interaction of the particles with hydrophobic walls (see Fig. 2a & b). We first repeat the classic experiments of floating objects on surfaces and find the attraction rate by releasing two confined unfueled particles and monitoring their separation distance. We test different release distances of 4 cm, to 10 cm (see Fig. 2c) where the Cheerios effect was observed for all these distances. (examples of unpowered attraction seen in Supplementary Video 2) As expected, regardless of the initial position, the distance between the two particles in different tests follows the same rapid attraction and almost identical separation when approaching one another (Fig. 2c).

The interaction scenarios for active particles are more complex. On the one hand, the Cheerios effect tends to attract the particles, while on the other hand, the active propulsion of each particle causes it to move inertially, primarily avoiding this attraction. As the particle activity decreases, the Cheerios effect becomes dominant, leading to an attraction between particles. One way to demonstrate this complex interaction between the particles is to constrain their mobility (see Supplementary Video 3). In an experimental setup, we fix one of the particles and allow limited mobility to the other by attaching it to a 3D-printed cantilever beam (see Fig. 2d). Initially, the particles are placed 10 cm apart and then manually and gradually (1 mm/s) brought closer together. We approach the static particle until reaching a critical distance, at which the cantilever beam deflects enough for the particles to make contact. This attractive force is based on the Cheerios effect, as explained above, mechanically derived from the contact angle at the water interface and the distance from other interfacial agents [38, 46]. When fueled, we observe the particle repelling from the adjacent particle, producing

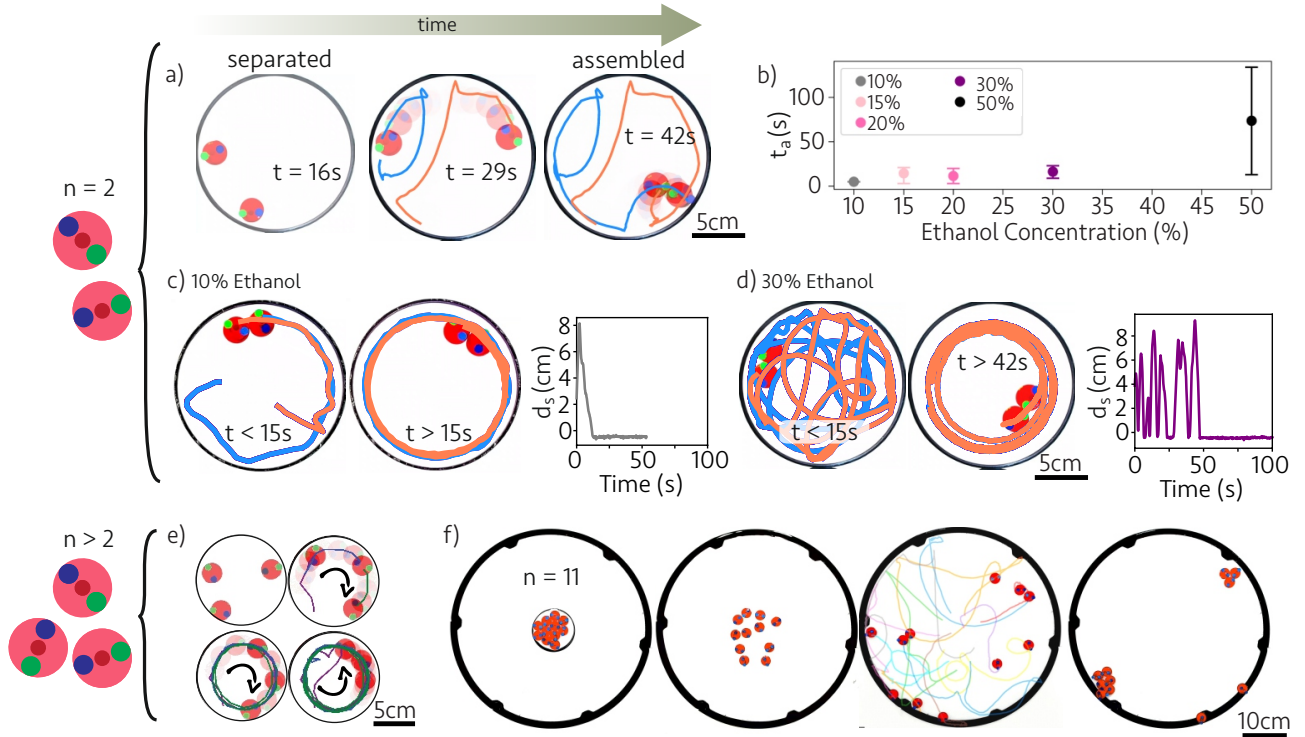


Fig. 3: Dynamics of multi-body active Cheerios systems. The top and bottom sections indicate the experiments with two or more particles, respectively. a) Example of 30% ethanol fueled particles into its working lifetime at $t = 16$ s, transit near the containment border at $t = 29$ s, and its assembled state at $t = 42$ s. b) Final assembly times for 10%, 15%, 20%, 30%, and 50% ethanol concentration fuels. c) Movement up to and after assembly while plotting separation distance (d_s) over time of 10% ethanol fuel motors. d) Movement up to and after assembly while plotting separation distance over time of 30% ethanol fuel motors. e) Three active particles in a confinement ring (ratio 6:1), transiting around containment, and aggregation to connected transit around the containment ring (see Supplementary Video 5). f) 11-particle system movement and aggregation using a special dual outlet design with initial fully compact configuration, release, motility, and eventual assembly into multi-particle groups (see Supplementary Video 6).

an observable deflection. We visualize the onset of Marangoni flow and repulsion with 0.1% fluorescein dye in a 30% ethanol-water mixture (see Fig. 2e). This interaction suggests that the fuel is hydrodynamically interacting with the static particle, likely indicating a force vector that induces deflection. Upon initial fueling, the deflection of the cantilever (and consequently the repulsive force) is at its maximum; this peak in deflection occurs immediately after fueling for all ethanol concentrations. This force diminishes over time, and once the activity weakens and the fuel is exhausted, the active motor rapidly contacts the static motor due to the dominating Cheerios attraction. It is worth noting that despite our efforts, the resolution and quality of force measurements using the 3D-printed cantilever were insufficient to quantify the propulsion and attraction force values. Alternative methods, such as those used in the work of Ho *et al.* [48], may be more effective.

Multi-motor Interaction & self-assembly

We proceed to observe and quantify the interaction between multiple powered, confined particles, where the competition between the previously discussed Cheerios effects and the activity of the particles governs the dynamics. The multi-body tests are performed using various hydrophobic ring diameters to investigate separation and assembly properties (see Fig. 3). The primary size ratio used was $\sim 7 : 1$ with a confinement ring (15 cm diameter) to particles (2.2 cm diameter). We release the particles directly next to one another with diametrically opposing outlets to ensure they have the greatest aggregate repulsive thrust. A typical example of a two-body system is shown in Fig. 3a. (also examples seen in Supplementary Video 4) In the early stages, Marangoni stresses and flows are strong; hence, the activity of the particles dominates, leading to free self-propelled motion. As the particles deplete their fuel, the Cheerios effects become stronger and eventually result in attraction and contact between the particles. The time at which this assembly occurs depends on the ethanol concentration. Generally, the higher the ethanol concentration (and the stronger the motility, as shown in Fig. 1f & g), the longer the assembly time, t_a .

Low ethanol concentrations do not create enough thrust or inertial momentum to separate the particles for more than several seconds. The particles operating at 15%, 20%, and 30% ethanol each have marginally longer contact times than those operating at 10% ethanol concentration. Surprisingly, the 50%-ethanol-fueled active Cheerios have a much broader range of contact times, from those similar to the order of a few seconds to nearly

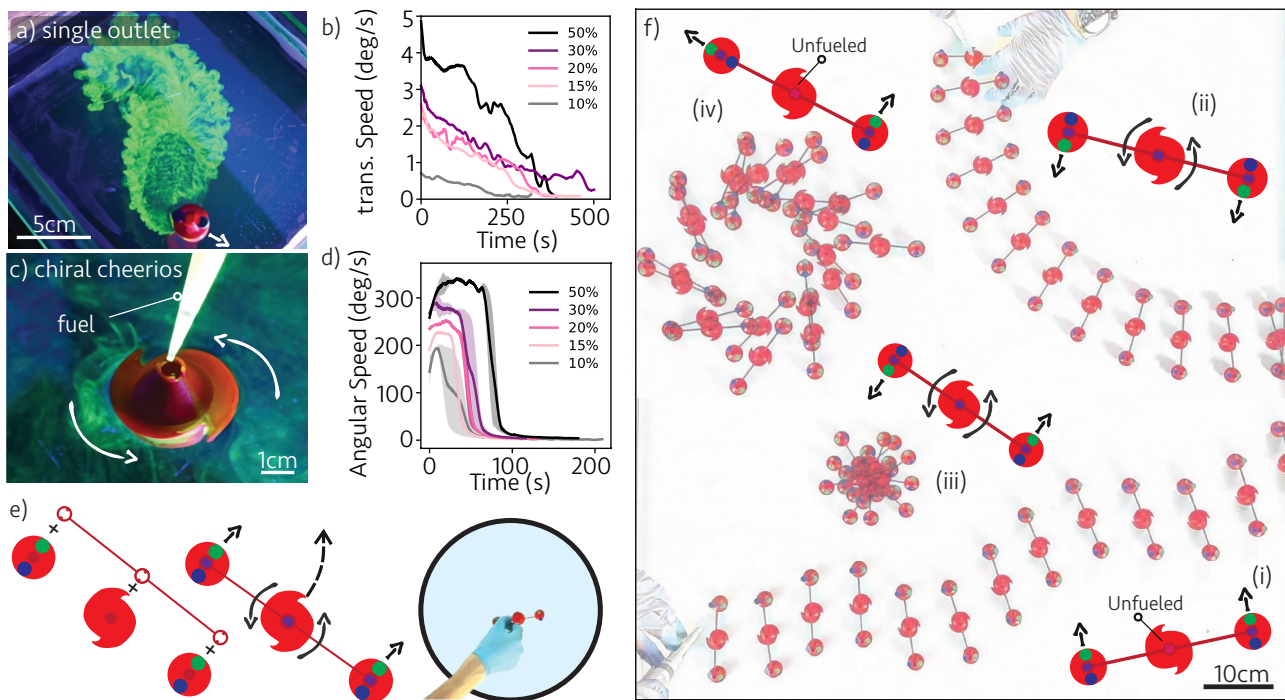


Fig. 4: Multiparticle construction for engineering propulsion direction. a) Single outlet design with fluorescent fuel. b) Average speed of single outlet particles for different ethanol concentration. c) Chiral particles with fluorescent fuel. d) Angular speed of chiral particles for different ethanol concentration. e) Schematics of modular construction. f) An array of different modular particle assemblies for (i) linear movement, (ii) curved motion, (iii) on-axis spinning, and (iv) off-axis spinning.

120 seconds. Note that at low motility regimes (see Fig. 3c for an example), the first contact made by the particles often leads to a permanent assembly. At high motility regimes, the inertial momentum prevents the particles from remaining in contact. Initially, the particles come into contact due to their momentum, carrying them into close proximity and even colliding (where the attractive forces are the strongest). Still, they will separate shortly after the collision due to high inertia. These phenomena are shown in Fig. 3d, where the particles transiently contact each other up to six times before being dominated by the attractive Cheerios effect when the velocity decreases and the lifetime of the particle reaches its fully assembled state. After the assembly, the two particles enter a circling trajectory at the ring border in almost all cases (see examples in Fig. 3c & d). This circling emerges when the particles assemble or repel each other in a self-reinforcing direction of motion around the perimeter, given sufficient fuel reserves. Note that no particular pattern was observed for the relative orientation of the particles upon assembly.

As we increase the number of active Cheerios, the dynamics of collective self-propulsion and self-assembly of particles become more complex. Examples of 3 and 11 particles are shown in Fig. 3e & f, respectively. The particles in the three-body system (Fig. 3e) initially expand radially from the center and proceed to transit the perimeter of the containment ring. The direction of circumvention appears to be random, but once established, the particles consistently follow the path in the same direction. (seen in Supplementary Video 5) Finally, we tested an 11-particle release using a different design with two diametrically opposite-positioned outlet holes that produce opposing thrust, creating an unstable quadrupolar flowfield that rapidly breaks the symmetry and allows the particle to travel transverse to the axis of the outlets (see Fig. 3e). Two outlets were used to separate the tightly packed particles due to the highly repulsive effects at the beginning of their lifetimes, necessary to overcome Cheerios attraction forces. Note that the two-outlet design has distinctly different motility characteristics from the original single-outlet design but demonstrates aggregation even in a much larger containment ring. Ultimately, when the particles' activities weaken, they assemble in small crystal structures and float in large groups of particles, which are collectively motile until they completely exhaust their fuel (see Supplementary Video 6).

The overall behavior of these systems with a large number of particles depends on various factors, including the design (*e.g.*, number and position of outlets and shape), confinement, ethanol concentration (Marangoni-stress), and clearly the number of particles. A complete parametric study of these factors is beyond the scope of this work. However, we emphasize that the combination of hydrodynamic interactions (flow and interfacial effects) and the stochastic characteristics of the multi-body active Cheerios makes it a significantly rich, albeit frugal, experimental system to explore collective active motions, with many details yet to be discovered. Furthermore, the system's flexibility allows for the design of active systems, a goal we will pursue in the next and final sections.

IV. CHIRAL PARTICLES AND MODULAR DESIGN WITH ACTIVE CHEERIOS

The use of 3D printers allows us to design particles with different motion characteristics. Here, we demonstrate this by first designing chiral active Cheerios and then presenting a modular design where various particles are mechanically linked to program different propulsion trajectories.

We use knowledge of directional thrust in round particles with one or more outlets (see Section II and Fig. 4a and b) to create another new particle. The design achieves a chiral particle using two outlets with semicircular interfacial cups to diffuse fuel tangentially to the particle body circumference (see Fig. 4c). Redirecting the fuel deposition and direction of thrust creates a moment on the particle using outlet force principles and an angular rotation that depends on ethanol concentration (see Fig. 4d). Higher ethanol concentrations result in greater maximum angular velocity and slightly longer lifetimes. The particle start with high angular velocity, which gradually diminishes, following characteristically shorter lifetimes than single-outlet motors mainly because two outlets in the chiral particle cause it to release its fuel more quickly.

Combining the single-outlet and chiral particle, we built rigid, mechanically-linked multi-particle networks for customized locomotion (see Fig. 4e and f). The constructs are made by connecting individual particles with thin 3D-printed linkages that lock onto the fuel tank inlets located on the tops of the particles. We affix three particles to a straight linkage, allowing the overall assembly to float and move within a large square water-basin container. The linkage spacing is similar to the motor diameter, which minimizes interaction with the fast flows exiting the outlets of individual particles. Hence, we can program a trajectory based on the Marangoni-induced force vectors. By combining each motor propulsion mechanism, we construct diagnostic assemblies to confirm the modularity of our linked active particles.

Besides designing the particles (and turning them on/off by fueling or not), we also use their orientation to create a variety of movement modes (see Fig. 4f). The motions can be categorized as linear, curved, on-axis spinning, and off-axis spinning. We create a predominantly linear trajectory across the containment tank by powering both single-outlet particles attached to the construct and orienting them in the same thrust direction (Fig. 4f-i). During linear translation, lateral fluctuation is likely due to the structure's higher inertia and complex drag profile, creating symmetry breaking during transit. We create an assemblage with a curved trajectory using a linear configuration with a powered central chiral particle. When all particles are powered, the chiral one imparts a moment onto the assembly, producing a turning motion (Fig. 4f-(ii)). By reorienting one of the single-outlet particles by 180° , we create an on-axis spinning assembly, where the reinforcing moment from the single-outlet side particles in the direction of the chiral particle's counterclockwise rotation forms a chiral assembly that spins on its own axis (Fig. 4f-iii). We then demonstrate an off-axis spinning design using a single-outlet particle propelling parallel and outward from the constructed chain with an inactive chiral motor. The perpendicular Marangoni propulsion forces from the single-outlet designs produce off-axis spinning behavior (see Fig. 4f-iv).

These basic demonstrations validate that single Marangoni-driven active particle systems can be scaled to larger, more predictable modular assemblies by showing each unique propulsion behavior and trajectory. Such designer systems can be improved and further developed in various ways, as we will briefly discuss in the following conclusions and outlook section.

V. CONCLUSION & OUTLOOK

This study demonstrates a straightforward yet effective approach to designing Marangoni-driven active particles that operate on a water surface, leveraging both the Marangoni and Cheerios effects to produce tunable motility and interaction patterns. The versatility of this system not only allows for precise control over particle behavior but also provides a simplified platform for studying complex collective dynamics. Such dynamics are analogous to those observed in natural systems, including ant rafts [37] and bacteria on surfaces [49, 50], where interactions at interfaces give rise to emergent phenomena. By offering insights into the interplay of forces and interactions, this system has the potential to deepen our understanding of these biological systems and inform the development of bio-inspired designs in active matter and soft robotics. Moreover, the present system provides access to less-studied hydrodynamic regimes, including inertial effects [51], making it a versatile tool for exploring new active matter behaviors. Besides ethanol concentration, one could also control the motility of the particles by the viscosity of the fuel or the liquid around it (see Appendix E). The experimental results also showcase other complex behaviors in multi-body systems, including phenomena such as active crystals [52, 53], where a cluster of active Cheerios co-translate and co-rotate, and weak self-avoidance [54, 55], where particles avoid previous trajectories at higher ethanol concentrations. Future studies could further explore the details of these features.

Designing active particles with various trajectories and also modular systems where particles of different characters are mechanically linked proves the flexibility of the present system. However, the design process for active Cheerios was primarily based on trial and error, but future work could benefit from integrating optimization

techniques to refine the design pipeline for greater precision and efficiency but also more practical trajectories. Additionally, machine learning could help identify optimal geometries and fuel compositions more systematically, improving both motility and stability. Furthermore, programmable fuel release mechanisms could enable longer and more complex trajectories, opening up possibilities for increasingly sophisticated interfacial navigation.

Throughout this article, we primarily adopted an exploratory approach with minimal reliance on theory. The experimental results presented here could greatly benefit from future theoretical investigations across various scales. At the single-particle scale, the interplay of physicochemical hydrodynamics near the outlet, symmetry-breaking, and (inertial) propulsion offers a fertile ground for exploration. The simplicity of the experiments further enables precise testing of these theories. For multibody systems, experimental findings could be complemented by a range of theoretical frameworks, from simplified active particle models based on Langevin-like equations to detailed simulations accounting for hydrodynamic interactions and surface deformability.

Finally, we would like to mention that beyond research applications, the simplicity and adaptability of this active particle system make it highly suitable for educational purposes. It offers a hands-on opportunity to teach fundamental concepts in Marangoni flow, flow visualization, active matter, and particle tracking. With real-time visual feedback, students can engage deeply with the principles underlying these phenomena, making this system a valuable tool for both experimental science and science education. Overall, this work establishes a foundation for further exploration of active and adaptive interfacial devices with potential applications in robotics, environmental sensing, and beyond.

ACKNOWLEDGMENTS

We thank the Technology Centre of the University of Amsterdam for their assistance with the experimental setup. We also thank Vera Horjus, Corentin Coulais, and Vatsal Sanjay for valuable discussions. MJ acknowledges support from the NWO grant no. OCENW.XS21.1.140. JKW acknowledges the support of the National Science Foundation Graduate Research Fellowship Program for support during the writing and submission of this article.

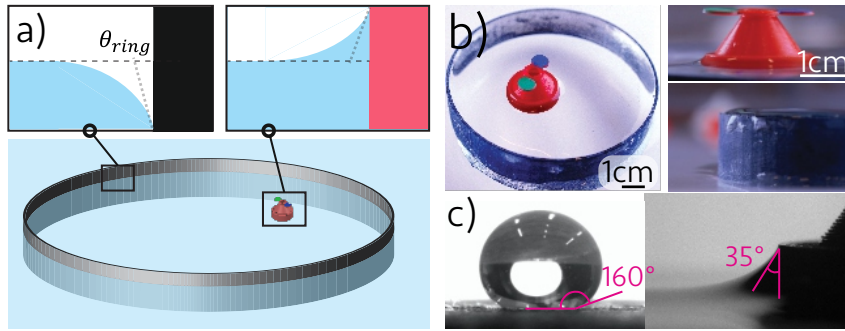


Fig. V.1: Contact angle for the motors and containment ring in a water basin. a) The black wall shows the cross-sectional version of the containment ring with a hydrophobic surface, while the red wall is the cross-sectional surface of the particle and a hydrophilic surface. b) Photograph of the particle and containment. c) Approximation of the contact angle from side images of a water droplet on a coated hydrophobic surface and the contact angle of the meniscus on an active Cheerios.

APPENDICES

APPENDIX A: 3D PRINTING

We print the particles using PLA (red Polylactic Acid Filament; Ultimaker, Utrecht, NL) fused-deposition modeling (Ultimaker 2+; Ultimaker, Utrecht, NL), due to its prevalence in extrusion-based printing for labs and classrooms. The containment ring is also 3D printed using PETG (Polyethylene terephthalate glycol) fused filament fabrication. We use the large 3D printed 45 cm diameter and 3 cm deep ring to perform far-field motility in a 6 cm deep rectangular water basin.

APPENDIX B: HYDROPHILIC PARTICLES AND HYDROPHOBIC WALLS

All of the printed materials are hydrophilic with a pronounced meniscus with a contact angle of $\sim 35^\circ$ on their surfaces when at the air-water interface (see Fig. V.1). We coat the containment ring with a super hydrophobic spray (NeverWet Multi-surface Spray; Rust-Oleum, Evanston, IL, U.S.). The hydrophobic ring has a contact angle of $\theta_{ring} \approx 160^\circ$, which prolonged motility with reduced structure-structure interaction between the Active Cheerios and the ring.

APPENDIX C: PROPULSION

The theory of propulsion for active Cheerios deserves a more complete analysis. Here, we aim to present a simplified picture by balancing estimated forces. The surface tension gradient generated at the particle's outlet leads to a mismatch between direct forcing on the particle and, hence, propulsion. The magnitude of this force can be estimated as $\Delta\gamma D_n$, where $\Delta\gamma$ is the difference between the surface tension on two sides and D_n is the nozzle diameter as a rough estimation of the length contact line force is acting on. The driving force should balance the drag force. The Reynolds number ($Re = \rho U_p D_p / \mu$, with ρ as the density, U_p as the particle velocity, and μ as the viscosity) is much larger than unity in most cases here. Hence, the drag force could be estimated as $\rho U_p^2 D_p^2$. This balance leads to $U_p \approx (\Delta\gamma D_n / \rho D_p^2)^{1/2} \sim \mathcal{O}(1 \text{ cm/s})$. On the other hand, the surface tension gradient at the outlet also leads to Marangoni flow. An estimation of fluid velocity at the nozzle may be achieved by balancing the Marangoni stresses $\Delta\gamma \mathcal{L}$, where \mathcal{L} is a characteristic length scale where surface tension gradient is acting. Inspecting the flow field around the particles, we see a region of fast flow near the nozzle (see fig 1c). Assuming the gradient of surface tension is negligible beyond this region and based on observation, we take $\mathcal{L} \approx D_p$. If we assume the Marangoni stress at the nozzle balances with the viscous stress of a thin layer near the interface approximated as $\mu U_e / \mathcal{H}$, with $\mathcal{H} \approx D_n$, we then arrive at nozzle velocity of $U_e \approx D_n \Delta\gamma / D_p \mu$. Finally, balancing the flow forces generated at the nozzle with the drag force, we arrive at $U_p \approx U_e D_n / D_p \sim \mathcal{O}(1 \text{ cm/s})$, which is the same order of magnitude as found from direct forcing on the contact line of the particle. Hence, in general, we expect both mechanisms to be involved in particle's propulsion. However, note that, for most results shown here, we estimate Marangoni flow stresses play a more pronounced role. Better estimation of particle velocity, as well as particle trajectories, requires more complete theoretical and computational study of active Cheerios.

APPENDIX D: INERTIAL EFFECTS

The particles are inertial throughout their lifetimes. In single outlet particles, this results in a phase difference between particle orientation and velocity direction (See Fig. V.2). This is shown by comparing the angle of

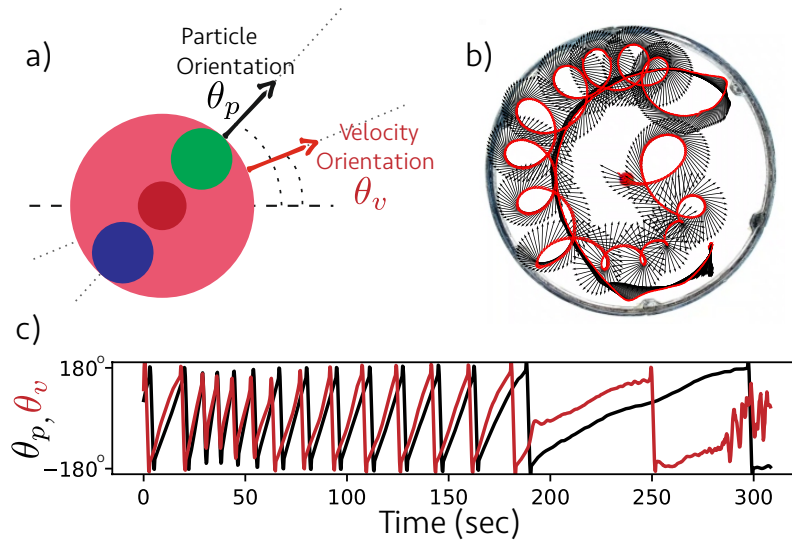


Fig. V.2: a) Identification of the angles θ_p and θ_v for the actual particle orientation (black) based on the geometrical location of the fuel outlet and the tracked velocity orientation (red). b) Example of particle and velocity orientation vector arrows plotted during the lifetime of a particle with 50% ethanol fuel. c) Variation of θ_p and θ_v .

particle orientation (black) and velocity direction (red). When the particle decays, the difference between the two vectors become apparent as the propulsive effects are less effective, and the orientation of the particle is then static due to reduced fuel.

APPENDIX E: VISCOSITY EFFECTS

Here, we report the results varying the fuel and reservoir liquid viscosity independently using glycerine. Glycerine is first added to the ethanol fuel to observe how the viscosity affects the particle lifetime, stabilizing and lowering the diffusion rate of the fuel (see Fig. V.3a). When using 50% glycerine - 50% ethanol, we get dramatically different qualitative and quantitative results. There is a clear velocity plateau at approximately 2.5 cm/s with a much more gradual decline to cessation. In this case, this shows that there are dramatically more consistent and prolonged lifetimes up to three times longer or death beginning at 750s. The lower ethanol also correlates to a lower overall average speed calculated for each particle. The velocity is dramatically lowered at lower ethanol percents, likely due to the severely impeded diffusion and more significant viscous dissipation. This informs us that future studies will investigate higher viscosity fuels to tune the inertial effects and achieve Stokesian swimmers if required.

In a different experiment, glycerine is added to the reservoir basin to evaluate the effects of viscosity in the basin on lifetime and velocity (see Fig. V.3b). These basin liquid tests show that The highest concentration of pure glycerine corresponds to the lowest velocity of all tests conducted. In general, we observe increased velocity and lifetimes when reducing the glycerine concentration in the basin, showing the higher viscous stresses on the particles. The glycerine water basin was largely unsuccessful in extending lifetimes or generating more linear trajectory paths. The lower performance is likely due to the reduced fuel diffusion efficacy on the reservoir surface and less Marangoni propulsion. The fuel likely diffuses too rapidly around the motor with inadequate force transfer, lowering velocity and acceleration.

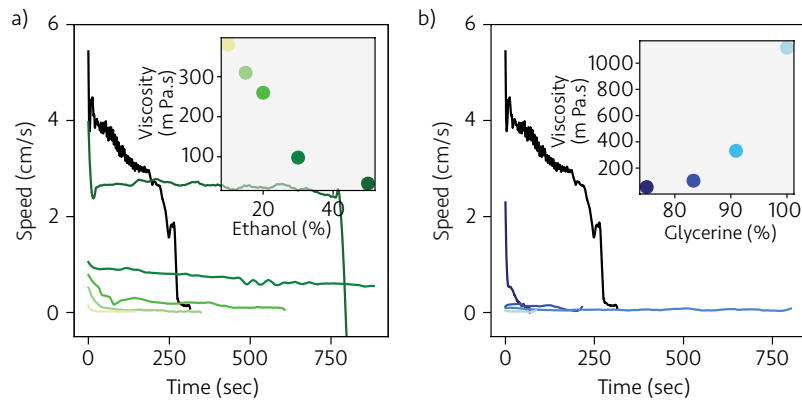


Fig. V.3: a) Traveling speed of particles with glycerine-ethanol fuel. The viscosities (inset) are measured with an Anton Paar 502 rheometer. b) Traveling speed of particles with ethanol solution as fuel, moving in a basin with water-glycerine solutions.

REFERENCES

- [1] X. Zhang, J. Zhao, Q. Zhu, N. Chen, M. Zhang, and Q. Pan, “Bioinspired aquatic microrobot capable of walking on water surface like a water strider”, *ACS applied materials & interfaces* **3**, 2630–2636 (2011).
- [2] J. Yuan and S. K. Cho, “Bio-inspired micro/mini propulsion at air-water interface: a review”, *Journal of mechanical science and technology* **26**, 3761–3768 (2012).
- [3] D. Feldmann, R. Das, and B.-E. Pinchasik, “How can interfacial phenomena in nature inspire smaller robots”, *Advanced Materials Interfaces* **8**, 2001300 (2021).
- [4] E. Rhee, R. Hunt, S. J. Thomson, and D. M. Harris, “Surferbot: a wave-propelled aquatic vibrobot”, *Bioinspiration & Biomimetics* **17**, 055001 (2022).
- [5] I. Ho, G. Pucci, A. U. Oza, and D. M. Harris, “Capillary surfers: wave-driven particles at a vibrating fluid interface”, *Physical Review Fluids* **8**, L112001 (2023).
- [6] D. Kim, C. J. Park, J.-S. Koh, and J. Ha, “Small-scale robots inspired by aquatic interfacial biolocomotion”, *MRS Bulletin* **49**, 148–158 (2024).
- [7] C. W. Shields and O. D. Velev, “The Evolution of Active Particles: Toward Externally Powered Self-Propelling and Self-Reconfiguring Particle Systems”, en, *Chem* **3**, 539–559 (2017).
- [8] X. Dong and M. Sitti, “Controlling two-dimensional collective formation and cooperative behavior of magnetic microrobot swarms”, en, *The International Journal of Robotics Research* **39**, 617–638 (2020).
- [9] J. W. Bush and D. L. Hu, “Walking on Water: Biolocomotion at the Interface”, en, *Annual Review of Fluid Mechanics* **38**, 339–369 (2006).
- [10] J. Deng, M. Molaei, N. G. Chisholm, T. Yao, A. Read, and K. J. Stebe, “Active colloids on fluid interfaces”, *Current Opinion in Colloid & Interface Science* **61**, 101629 (2022).
- [11] V. Pimienta and C. Antoine, “Self-propulsion on liquid surfaces”, *Current opinion in colloid & interface science* **19**, 290–299 (2014).
- [12] L. Scriven and C. Sternling, “The marangoni effects”, *Nature* **187**, 186–188 (1960).
- [13] J. Thomson, “Xlii. on certain curious motions observable at the surfaces of wine and other alcoholic liquors”, *The London, Edinburgh, and Dublin Philosophical Magazine and Journal of Science* **10**, 330–333 (1855).
- [14] C. Marangoni, *Sull’espansione delle gocce d’un liquido galleggianti sulla superficie di altro liquido* (Fratelli Fusi, 1865).
- [15] S. Thutupalli and S. Herminghaus, “Tuning active emulsion dynamics via surfactants and topology”, *The European Physical Journal E* **36**, 1–10 (2013).
- [16] K. Dietrich, N. Jaensson, I. Buttinoni, G. Volpe, and L. Isa, “Microscale Marangoni Surfers”, en, *Physical Review Letters* **125**, arXiv:2005.06811 [cond-mat], 098001 (2020).
- [17] B. V. Hokmabad, R. Dey, M. Jalaal, D. Mohanty, M. Almukambetova, K. A. Baldwin, D. Lohse, and C. C. Maass, “Emergence of Bimodal Motility in Active Droplets”, en, *Physical Review X* **11**, 011043 (2021).
- [18] M. Wittmann, M. N. Popescu, A. Domínguez, and J. Simmchen, “Active spheres induce marangoni flows that drive collective dynamics”, *The European Physical Journal E* **44**, 1–11 (2021).
- [19] M. Bourgoïn, R. Kervil, C. Cottin-Bizonne, F. Raynal, R. Volk, and C. Ybert, “Kolmogorovian Active Turbulence of a Sparse Assembly of Interacting Marangoni Surfers”, en, *Physical Review X* **10**, 021065 (2020).
- [20] D. Boniface, C. Cottin-Bizonne, R. Kervil, C. Ybert, and F. Detcheverry, “Self-propulsion of symmetric chemically active particles: point-source model and experiments on camphor disks”, *Physical Review E* **99**, 062605 (2019).
- [21] Y. Matsuda, K. Ikeda, Y. Ikura, H. Nishimori, and N. J. Suematsu, “Dynamical Quorum Sensing in Non-Living Active Matter”, en, *Journal of the Physical Society of Japan* **88**, 093002 (2019).
- [22] Y. Hirose, Y. Yasugahira, M. Okamoto, Y. Koyano, H. Kitahata, M. Nagayama, and Y. Sumino, “Two floating camphor particles interacting through lateral capillary force”, en, *Journal of the Physical Society of Japan* **89**, arXiv:1909.00545 [cond-mat, physics:nlin], 074004 (2020).
- [23] Y. Matsuda, N. J. Suematsu, H. Kitahata, Y. S. Ikura, and S. Nakata, “Acceleration or deceleration of self-motion by the marangoni effect”, *Chemical Physics Letters* **654**, 92–96 (2016).

- [24] H. Nishimori, N. J. Suematsu, and S. Nakata, “Collective behavior of camphor floats migrating on the water surface”, *Journal of the Physical Society of Japan* **86**, 101012 (2017).
- [25] B. Kwak, S. Choi, J. Maeng, and J. Bae, “Marangoni effect inspired robotic self-propulsion over a water surface using a flow-imbibition-powered microfluidic pump”, en, *Scientific Reports* **11**, 17469 (2021).
- [26] S. W. Song, S. Lee, J. K. Choe, A. C. Lee, K. Shin, J. Kang, G. Kim, H. Yeom, Y. Choi, S. Kwon, *et al.*, “Pen-drawn marangoni swimmer”, *Nature Communications* **14**, 3597 (2023).
- [27] S. Sur, N. Uvanovic, H. Masoud, and J. P. Rothstein, “The effect of shape on the motion and stability of marangoni surfers”, *Journal of fluids engineering* **143**, 011301 (2021).
- [28] C. Renney, A. Brewer, and T. J. Mooibroek, “Easy demonstration of the marangoni effect by prolonged and directional motion: “soap boat 2.0””, *Journal of Chemical Education* **90**, 1353–1357 (2013).
- [29] M. L. Timm, S. J. Kang, J. P. Rothstein, and H. Masoud, “A remotely controlled marangoni surfer”, *Bioinspiration & biomimetics* **16**, 066014 (2021).
- [30] S. Tsuchitani, T. Ikebe, H. Miki, and K. Kikuchi, “Electric field control of propulsion force of a boat driven by chemical marangoni effect”, *Colloids and Surfaces A: Physicochemical and Engineering Aspects* **592**, 124570 (2020).
- [31] I. Tiwari and P. Parmananda, “How to capture active marangoni surfers”, *Soft Matter* **19**, 2710–2715 (2023).
- [32] C. Renney, A. Brewer, and T. J. Mooibroek, “Easy Demonstration of the Marangoni Effect by Prolonged and Directional Motion: “Soap Boat 2.0””, en, *Journal of Chemical Education* **90**, 1353–1357 (2013).
- [33] D. Ivanov and S. Nikolov, “Molecular engine boat”, en, *Physics Education* **54**, 045006 (2019).
- [34] L. J. Burton, N. Cheng, C. Vega, J. Andrés, and J. W. M. Bush, “Biomimicry and the culinary arts”, en, *Bioinspiration & Biomimetics* **8**, 044003 (2013).
- [35] L. L. Gutierrez-Martinez and M. Sandoval, “Inertial effects on trapped active matter”, *The Journal of Chemical Physics* **153** (2020).
- [36] A. P. Antonov, L. Caprini, A. Ldov, C. Scholz, and H. Löwen, “Inertial active matter with coulomb friction”, *Physical Review Letters* **133**, 198301 (2024).
- [37] H. Ko, M. Hadgu, K. Komilian, and D. L. Hu, “Small fire ant rafts are unstable”, *Physical Review Fluids* **7**, 090501 (2022).
- [38] D. Vella and L. Mahadevan, “The “Cheerios effect””, en, *American Journal of Physics* **73**, 817–825 (2005).
- [39] G. Vazquez, E. Alvarez, and J. M. Navaza, “Surface Tension of Alcohol Water + Water from 20 to 50 .degree.C”, en, *Journal of Chemical & Engineering Data* **40**, 611–614 (1995).
- [40] B. A. Grzybowski and G. M. Whitesides, “Dynamic aggregation of chiral spinners”, *Science* **296**, 718–721 (2002).
- [41] S. Li, T. V. Phan, G. Wang, R. Khuri, J. W. Wilson, R. H. Austin, and L. Liu, “Memory of elastic collisions drives high minority spin and oscillatory entropy in underdamped chiral spinners”, *Communications Physics* **7**, 136 (2024).
- [42] J.-W. Barotta, S. J. Thomson, L. F. Alventosa, M. Lewis, and D. M. Harris, “Bidirectional wave-propelled capillary spinners”, *Communications Physics* **6**, 87 (2023).
- [43] C. Scholz, A. Ldov, T. Pöschel, M. Engel, and H. Löwen, “Surfactants and rotelles in active chiral fluids”, en, *Science Advances* **7**, eabf8998 (2021).
- [44] G. Bradski, “The OpenCV Library”, *Dr. Dobb’s Journal of Software Tools* (2000).
- [45] D. B. Allan, T. Caswell, N. C. Keim, C. M. van der Wel, and R. W. Verweij, *Soft-matter/trackpy: v0.6.1*, version v0.6.1, Feb. 2023.
- [46] M. Nicolson, “The interaction between floating particles”, in *Mathematical proceedings of the cambridge philosophical society*, Vol. 45, 2 (Cambridge University Press, 1949), pp. 288–295.
- [47] I. B. Liu, N. Sharif-Mood, and K. J. Stebe, “Capillary assembly of colloids: interactions on planar and curved interfaces”, *Annual Review of Condensed Matter Physics* **9**, 283–305 (2018).
- [48] I. Ho, G. Pucci, and D. M. Harris, “Direct measurement of capillary attraction between floating disks”, *Physical Review Letters* **123**, 254502 (2019).
- [49] J. Deng, M. Molaei, N. G. Chisholm, and K. J. Stebe, “Motile bacteria at oil–water interfaces: pseudomonas aeruginosa”, *Langmuir* **36**, 6888–6902 (2020).
- [50] J. Panich, E. M. Dubebout, N. Wadhwa, and D. F. Blair, “Swashing motility: a novel propulsion-independent mechanism for surface migration in salmonella and e. coli”, *bioRxiv* (2024).
- [51] D. Klotsa, “As above, so below, and also in between: mesoscale active matter in fluids”, *Soft matter* **15**, 8946–8950 (2019).
- [52] A. P. Petroff, X.-L. Wu, and A. Libchaber, “Fast-moving bacteria self-organize into active two-dimensional crystals of rotating cells”, *Physical review letters* **114**, 158102 (2015).
- [53] T. H. Tan, A. Mietke, J. Li, Y. Chen, H. Higinbotham, P. J. Foster, S. Gokhale, J. Dunkel, and N. Fakhri, “Odd dynamics of living chiral crystals”, en, *Nature* **607**, 287–293 (2022).
- [54] K. Daftari and K. A. Newhall, “Self-avoidant memory effects on enhanced diffusion in a stochastic model of environmentally responsive swimming droplets”, *Physical Review E* **105**, 024609 (2022).
- [55] T. Albers, S. Delnoij, N. Schramma, and M. Jalaal, “Billiards with spatial memory”, *Physical Review Letters* **132**, 157101 (2024).